



Mycosynthesis of highly fluorescent selenium nanoparticles from *Fusarium oxysporum*, their antifungal activity against black fungus *Aspergillus niger*, and in-vivo biodistribution studies

Sk Najrul Islam¹ · Syed Mohd Adnan Naqvi¹ · Azam Raza¹ · Amit Jaiswal² · Akhilesh K. Singh² · Manish Dixit² · Atul Barnwal² · Sanjay Gambhir² · Absar Ahmad¹

Received: 30 May 2022 / Accepted: 26 September 2022 / Published online: 5 October 2022
© King Abdulaziz City for Science and Technology 2022

Abstract

In the past few years, photo-luminescent inorganic materials have been studied extensively as fluorescent sensors, and diagnostic and bioimaging tools. The assessment of photoluminescence (PL) properties of selenium nanoparticles (Se NPs), especially mycosynthesized Se NPs, is still in its infancy. Herein, we have biosynthesized highly dispersed fluorescent Se NPs (42 nm) using endophytic fungus *Fusarium oxysporum*, and fully characterized them using sophisticated instruments like TEM, XRD, UV–Vis spectrophotometer, FTIR, and PL spectrometer. To determine the therapeutic efficacy and side effect profiles, these crystalline Se NPs were radiolabeled with technetium-99m (^{99m}Tc) and their biodistribution and renal clearance times were investigated in the normal Wister rat. The results showed that these Se NPs may be useful for targeting the lungs and liver dysfunction as significant accumulation of these NPs was observed in the liver (approx. $19.47 \pm 4\%$) and lungs (at $6 \pm 1\%$) after 10 min of post-injection. Quick circulation and the presence of Se NPs in kidney ($3.8 \pm 2\%$) also suggested the easy excretion of these NPs from the body through urinary tract. Furthermore, the antioxidant activity of Se NPs (IC₅₀, 159.5 µg/mL) has been investigated using DPPH free radical scavenging assay with scavenging efficacy of 80.4% where ascorbic acid (IC₅₀, 5.6 µg/mL) was used as a positive control. Additionally, the microscopic study of the inhibition zone encircled around Se NPs confirmed their strong antifungal and antispore activity against the black fungus *Aspergillus niger*.

Keywords Antifungal · *Aspergillus niger* · Biodistribution · Fluorescent · *Fusarium oxysporum* · Selenium nanoparticles

Introduction

Fluorescent nanoparticles and their surface functionalization have been receiving great scientific acclaim in the field of biomedical science as the biological traits and effects of nanoparticles can be easily changed by straightforward surface modification (He et al. 2019; Sanità et al. 2020; Jung and Neuman 2021). However, this modification typically involves the use of harmful chemicals for capping, which

often limits their applications in healthcare (Sukhanova et al. 2018). Thus, the biological approaches for nanoparticle synthesis are being adopted to overcome these toxicity issues as the biosynthesized nanoparticles are highly stable, water dispersible, and capped by nontoxic phytochemicals or natural protein molecules (Mukherjee et al. 2001; Shankar et al. 2003; Sudhasree et al. 2014; Zhang et al. 2021). Our group has done pioneering work in the biosynthesis of biomedically important nanomaterials using fungi, bacteria, and plant extract (Ahmad et al. 2003, 2004, 2007; Syed and Ahmad 2012; Islam et al. 2021a). The fungi are referred to as a "biofactory" for producing NPs, because this process is highly scalable, controllable, and inexpensive. The fungi-based bio-inspired method is better than the conventional biosynthesis approaches in terms of cost and reproducibility, since plant-based biosynthesis is geographically and seasonally variable, while bacterial biosynthesis requires expensive, sophisticated equipment for NPs' separation and

✉ Absar Ahmad
aahmad786in@gmail.com

¹ Interdisciplinary Nanotechnology Centre (INC), Z. H. College of Engineering and Technology, Aligarh Muslim University, AMU, Aligarh, UP 202002, India

² Department of Nuclear Medicine, Sanjay Gandhi Post Graduate Institute of Medical Sciences (SGPGIMS), Lucknow, UP 22014, India

purification. Nowadays, biosynthesized Se NPs become a promising material in healthcare, indicating significant effectiveness as an anticancer (Cruz et al. 2019; Vahidi et al. 2020), antimicrobial, and antioxidizing agent (Korde et al. 2020). Although several studies on the biosynthesis of Se NPs utilizing bacteria (Wadhvani et al. 2016; Ashengroph and Hosseini 2021; Bulgarini et al. 2021), fungi (Wadhvani et al. 2016; Abu-Elghait et al. 2021), and algae (Tehrani et al. 2020) have been published, little is known about their photoluminescence properties, especially for mycosynthesized Se NPs. In all the previous studies, the capability of saprophytic fungi has been investigated for the bio-reduction of selenite into Se NPs. Herein, we have biosynthesized Se NPs from the salt selenium (IV) chloride using the endophytic fungus *Fusarium oxysporum*, a well-known, important source of different enzymes that have various applications in biotechnology and nanomaterial synthesis (Ibrahim et al. 2021).

The in-vivo biodistribution study of different NPs has attracted a lot of attention in preclinical research to understand the therapeutic effectiveness, toxicity, and interactions between organs with nanoparticles (Khan et al. 2014; Nambangchang 2019; Yuan et al. 2019). Huang et al. reported chirality-dependent biodistribution of glutathion@Se NPs with the preferential accumulation of L-glutathion@Se NPs in the liver, spleen, and pancreas (Huang et al. 2020). Similar findings were made in another investigation, which discovered that Se NPs accumulated in the liver and kidney after being administered orally, with no detrimental effects on biochemical and hematologic indicators (Chandramohan et al. 2021). Radiolabel vitamin C-coated Se NPs were also reported to have poor physiochemical stability (Korany et al. 2020). As the NPs with different compositions and morphologies show distinct affinities toward various organs, we explored the biodistribution study of fluorescent Se NPs (mycosynthesized) capped with natural proteins, in normal Wister rat to figure out the effect of capping proteins in the biodistribution of Se NPs (Li and Huang 2008; Wei et al. 2018). When the biomass of the fungus *Fusarium oxysporum* is suspended in sterilized double distilled water, it releases various enzymes and proteins into the water. Our group previously reported that the enzyme with a molecular weight of 44-kilodalton was responsible for the enzymatic reduction of precursor ions (Kumar et al. 2007) while low molecular weight protein (13- kilodalton) capped the synthesized nanoparticles (Khan and Ahmad 2014). In this study, we have also confirmed the presence of capping protein using UV-visible and FTIR spectrometer, while residual phytochemicals were washed out using centrifugation. Parallely, we have investigated the antioxidant activity of protein-capped fluorescent Se NPs. In the present COVID-19 pandemic situation, *Aspergillus* infection caused by the black fungus *Aspergillus niger* has become life-threatening

to immune compromised SARS-CoV-2-infected patients in intensive care units. A recent study exposed that one-third of the ventilated COVID-19 patients also had *Aspergillus* infections and roughly 50% of them died. Thus, different antifungal drugs have been used as a preventive measure for seriously ill COVID-19 patients even if they have not tested positive for fungal infection. The excessive use of these drugs increases antifungal drug resistance and is no longer effective for fungal inhibition. In view of the public health and current pandemic situation, our group has biosynthesized Se NPs and unveiled their antifungal and antispore activity against the black fungus *Aspergillus niger*.

Materials and methods

Chemicals

The analytical reagent-grade chemicals and reagents were commercially accessible and utilized as delivered without further refining. Selenium tetrachloride (SeCl_4) that was used for the biosynthesis of fluorescent Se NPs was procured from Sigma-Aldrich, while fungal media components were obtained from Hi-media (Malt extract, Yeast extract, Peptone) and Qualigens (D-glucose). Technetium-99m was obtained as pertechnetate elute from $^{99}\text{Mo}/^{99\text{m}}\text{Tc}$ generator which was acquired from the SDS Life Sciences Pvt Ltd. Whatman paper No.1 sheets were obtained from Merck (Darmstadt, Germany). Equipment ANaI (TI) γ -ray scintillation counter (Scaler-Ratemeter SR7 model, UK) was utilized to detect the radioactivity. A high-powered sonicator was employed for the encapsulation process. Additionally, 2,2-diphenyl-1-picrylhydrazyl (DPPH) and ascorbic acid were purchased from Alfa Aesar and SD-fine, respectively, for free radical scavenging assay.

Maintenance and growth condition of fungal strain

The strain of endophytic fungus *Fusarium oxysporum* was maintained on potato dextrose agar (PDA) slants by monthly sub-culturing and stored in the B.O.D. incubator at 25 °C. The preserved strain of the fungus *Fusarium oxysporum* was then transferred into 100 mL aqueous MGY medium which was prepared in 500 mL Erlenmeyer flask by adding malt extract (0.3%), glucose (1%), yeast extract (0.3%), and peptone (0.1%). Then, the mycelia-containing flasks were kept on a rotary shaker (200 rpm) at 25 °C. The fungal strains started to grow at pH 7–9, and after 96 h of continuous shaking, the biomass was separated from the culture medium by centrifugation (7000 rpm, 15 min) at 15 °C. Then, the separated biomass was washed thrice with sterile distilled water for further use.

Biosynthesis of fluorescent Se NPs

Biosynthesis of Se NPs was carried out by adding approximately 20 gm of biomass into 100 mL of freshly prepared aqueous SeCl_4 solution (2 mM) in a 500 mL sterilized Erlenmeyer flask. The reaction mixture was then placed on the rotary shaker (200 rpm) at room temperature. After 72 h of reaction completion, the mycelia were separated from the respective medium by a simple filtration method. The obtained red filtrate containing highly dispersed fluorescent Se NPs was lyophilized and stored as a powder for further investigation.

Techniques used for characterization of Se NPs

The UV–Vis–NIR spectrophotometer (Cary 5000) was used in the wavelength range of 200–800 nm to investigate the absorbance of mycosynthesized Se NPs. To examine the characteristic bond vibration frequencies, the Fourier transform infrared (FTIR) spectrometry (PerkinElmer) was performed in the wavelength range of 400–4000 cm^{-1} . Using photoluminescence (PL) spectroscopy, fluorescence behavior of Se NPs was explored. The shape, size, and average particle-size distribution of Se NPs were surveyed using Transmission Electron Microscopy (TEM, JEM-JEOL, JAPAN). To obtain Transmission Electron Micrographs (TEM images), the Se NPs were dropcasted on carbon-coated copper grid and show under the TEM operating at a 100,000 \times magnification. Finally, X-ray powder diffraction (XRD) technique (Rigaku X-ray Diffractometer) and selected area electron diffraction (SAED) were used to confirm the crystallinity and unit lattice parameters of Se NPs. XRD diffractogram of lyophilized Se nanopowder was measured in the 2θ range of 20°–80° with a step size of 0.04° and a time of 5 s per step at 40 kV voltage and a current of 30 mA. For SAED analysis, same Se NPs-loaded carbon-coated copper grid was used for the recording of SAED pattern at an angular magnification of 0.001 nm per degree.

Radiolabeling of selenium nanoparticles

In a one-vial synthesis procedure, $^{99\text{m}}\text{Tc}$ -Se NPs were prepared in a vial by adding materials at 25 °C. Selenium nanoparticles were added to a dry and clean vial and followed by 100 μL of a fresh elute $^{99\text{m}}\text{Tc}$ as $\text{Na}^{99\text{m}}\text{TcO}_4$ in saline with about 200–370 MBq activity. The vial was shaken well till all suspense was mixed well, and finally, the reaction mixture was stirred for 25 min at 40 °C. The final volume of the prepared radioactive kit was 2.1 mL.

Radiochemical yield of $^{99\text{m}}\text{Tc}$ -Se NPs

The radiochemical yield percentage of $^{99\text{m}}\text{Tc}$ -Se NPs was determined by instant thin-layer chromatography (ITLC, 12 cm long and 1 cm wide), marked at a distance of 2 cm from the lower end and lined into sections 1 cm each up to 10 cm. A few drops from the mixture were spotted using a hypodermic syringe, and then, the strip was developed in an ascending manner in a jar using only acetone as a developing solvent. After complete development, the strips were dried and cut into fragments 1 cm each, and then, the sections were counted by NaI (TI) γ -ray scintillation counter for measuring radioactivity. The percentage of radiochemical yield was calculated by division of the radioactivity of radiolabeled nanoparticles ($^{99\text{m}}\text{Tc}$ -Se NPs) by the total activity multiplied by 100. The radiolabeling efficiency was in the range of > 95% and stability was measured at different points of time, at both solution conditions and physiological states.

In-vitro stability study

The in-vitro stability of $^{99\text{m}}\text{Tc}$ -Se NPs formulation was estimated to investigate the radiochemical tolerance in physiological conditions. Exactly 0.1 mL of the final preparation of $^{99\text{m}}\text{Tc}$ -Se NPs (1 μCi /500 μL) was incubated with 0.9 mL of Human Serum albumin (pH = 7.4) for different time intervals (0, 100, 200, 350, 1440 min) at 37 °C. The radiochemical yields were determined by the above-described ITLC method at different time intervals.

In-vivo biological studies

The in-vivo preliminary evaluation was evaluated in groups of normal Wistar rat at different point intervals. Exactly, 75 μL having 11–14 MBq of the radiolabeled NPs was intravenous (I.V.) injected in the tail vein. For each group, the rats were anesthetized and then weighed at 10, 60, 120 min and 6 h post-injection (p.i.). All organs were extracted, flushed with saline, and weighed, and their radioactivity was estimated using a well-type NaI gamma counter where the background was excluded. The percentage injected activity per gm of tissues (%ID/g) was estimated using the formula given below and the tissue uptakes were evaluated.

$$\% \text{ID} / \text{g} = \frac{\text{Counts per gram or gan}}{\text{Counts dose given}} \times 100$$

Antifungal, antispurulant, and antioxidant activity

The antifungal and antispurulant activity of Se NPs has been investigated against the black fungus *Aspergillus niger* by

the disc diffusion method. Initially, the stock solution of Se NPs having a concentration of 8 mg/mL was prepared and subsequently diluted to 4, 2, 1, 0.5, and 0.25 mg/mL by adding distilled water. 30 μ L from each prepared solution (containing 240, 120, 60, 30, 15, and 7.5 μ g) were loaded onto sterile discs (A, B, C, D, E, and F, respectively) and placed on PDA petri plates having the spores of *Aspergillus niger*. Fluconazole 10 μ g (mcg) antifungal disc (H) was used as positive control, while 30 μ L water (G) was considered a negative control. To determine the anti-sporulation activity of Se NPs, the hyphal growth of fungus *Aspergillus niger* was closely monitored using an optical microscope as microscopic visualization is considered the best method to assess sporulation.

2,2-Diphenyl-1-picrylhydrazyl (DPPH) radical scavenging assay was carried out for the assessment of the antioxidant activity of fluorescent Se NPs. The absorbance of Se NPs aliquots (1000, 500, 250, 125, 62.50, and 31.25 μ L/mL) was measured at 517 nm. The different concentrations of these aliquots were prepared by the addition of 1 mL Se NPs solution into 3 mL of methanolic DPPH solution (0.02 mM). The radical scavenging capacity of Se NPs in reference with standard ascorbic acid (100, 50, 25, 12.5, 6.25, and 3.125 μ L/mL) and methanol (negative control) was evaluated followed by the IC₅₀ value determination. The percentage (%) of inhibition for Se NPs and ascorbic acid were calculated by applying the following formula:

$$\% \text{ Inhibition} = \frac{\text{Abs}(C) - \text{Abs}(T)}{\text{Abs}(C)} \times 100$$

where Abs(C) and Abs(T) represent absorbance of the control sample and test sample, respectively.

Results and discussion

Nanoparticles characterization

The initial confirmation of Se NPs formation was obtained through visual observation that showed a color change from yellowish white to clear red during the reaction. After completion of the reaction, the red filtrate was analyzed by UV–visible spectroscopy. The strong absorption peak observed at 265 nm was due to surface plasmon resonance (SPR) of protein-capped Se NPs (Fig. 1a), while the absorption maxima were red-shifted at 276 nm (Fig. 1b) when mycosynthesized Se NPs were calcined at 200 °C (Kokila et al. 2017; Mellinas et al. 2019). The shifting of absorption maxima to a higher wavelength was attributed to the degradation of protein molecules from the surface of Se NPs.

The visualization of intense sky-blue fluorescence and the PL spectra confirm the photo-luminescent behavior of biogenic Se NPs (Fig. 1c). The highly intense emission peak that appeared at 360 nm (excited at 250 nm) was characterized by natural protein-capped biogenic Se NPs, which was not detected for chemogenic nano Se (Prasanth and Sudarsanakumar 2017; Piacenza et al. 2020). It was also observed that when biogenic Se NPs' solution was excited at 280 nm, the wide red-shifted emission peak appeared in the wavelength range of 390–420 nm. The redshift of excitation-dependent emission spectra can be attributed to the non-homogeneous size distribution as the PL properties of NPs are highly dependent on NPs size and capping agent (Piacenza et al. 2020).

Most importantly, TEM images (Fig. 2a and b) of bio-fabricated Se NPs were captured to confirm the shape and size of NPs. The captured electron micrograph demonstrated that the synthesized NPs are spherical with an

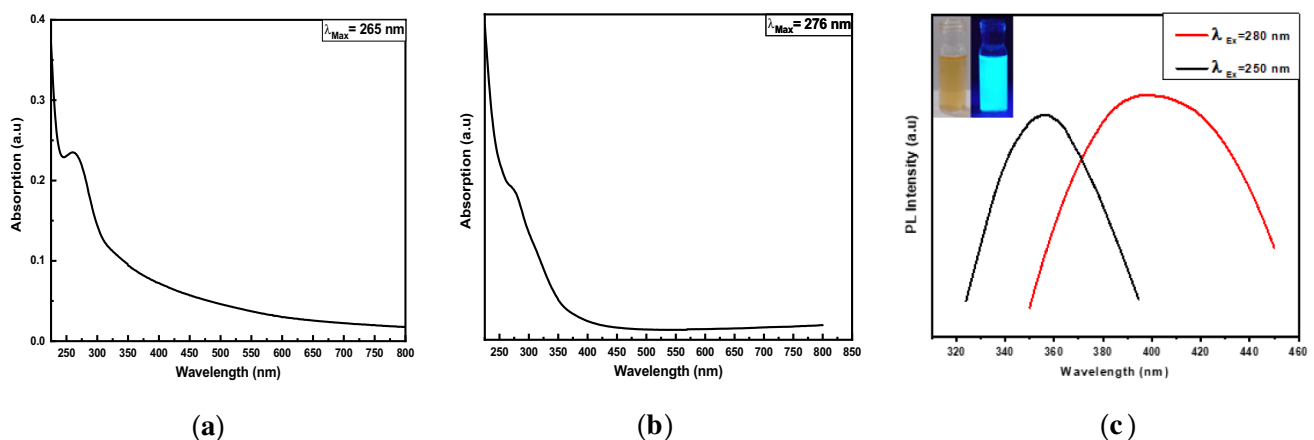


Fig. 1 UV–Vis spectra of **a** as-synthesized Se NPs and **b** after calcination at 200 °C. **c** Photoemission spectra of biosynthesized Se NPs correspond to the excitation wavelength of 250 and 280 nm

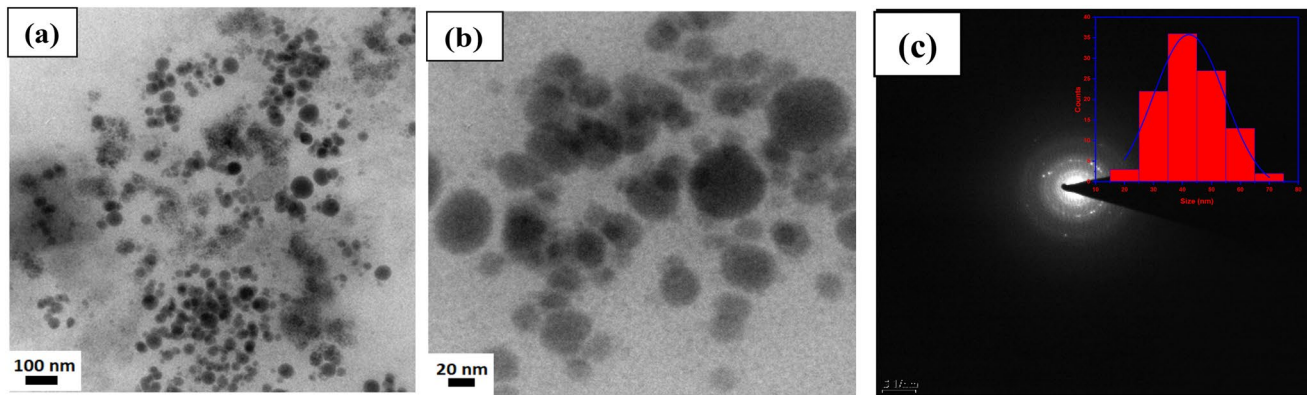


Fig. 2 TEM images (a, b) of biosynthesis Se NPs. These images presenting spherical morphology of Se NPs with variable sizes (c) SAED pattern incorporated with particle-size distribution histogram.

The randomly dotted ring in SAED pattern indicating the polycrystalline nature of Se NPs, while particle-size distribution histogram exploring the average particle diameter of 42 nm

average particle size of 42 nm, whereas the SAED pattern (Fig. 2c) confirmed the crystalline phase of Se NPs.

Further powder X-ray diffractometer (XRD) was performed to identify the crystallographic structure of mycosynthesized Se NPs. Figure 3a shows the diffraction pattern of as-synthesized Se NPs. The sharp and intense peaks appearing at 2θ angles of 27.31° , 30.74° , 39.35° , 49.05° , 57.45° , 65.47° , and 72.78° were indexed as (101), (011), (101), (110), (021), (012), and (120) planes conforming the hexagonal phase of Se NPs with space group P3121 (81.6%) and R3-MH (18.4%) (Ref. Pattern: 98-007-8796, 98-009-2700) (Islam et al. 2022).

Fourier transform infrared spectroscopy (FTIR) was executed to investigate the bond vibration frequencies associated with protein-capped Se NPs. The peaks that appeared at 3415 , 2947 , 1630 , 1520 , 1395 , and 1070 cm^{-1} in the FTIR spectrum (Fig. 3b.) are the characteristic peaks of proteins, whereas the peak observed at 530 cm^{-1} is due to the Se–Se bond vibration (Khiralla and El-Deeb 2015; Qian et al. 2017). The intense peaks at 3415 and 2947 cm^{-1} are identified for stretching vibration of O–H (alcohol) and N–H (amines). The sharp peaks obtained at 1630 and 1520 cm^{-1} correspond to amide I (N–C=O-stretching mode) and amide II (N–H bending mode), which are the main two characteristic peaks of proteins (Islam et al. 2021b), while the remaining two absorption band appeared at 1395 and 1070 cm^{-1} may be assigned to C–O-stretching mode (Khiralla and El-Deeb 2015).

Figure 4a and b shows the stability of the radiolabeled nanoparticles at room temperature while keeping the radioactivity at physiological saline and human serum albumin solution, respectively, and assessing its stability using ITLC method at different time points. The result showed that the Se NPs was chelated excellently with the metallic radionuclide ($^{99\text{m}}\text{Tc}$) at physiological pH range or at human serum albumin environment.

The NPs synthesized in this study are within the size range for biodistribution and no external capping agents were incorporated during synthesis.

Data in Fig. 5a and b showed that radiolabeled nanoparticle is well distributed as the maximum percentage injected dose per gm organ (% ID/g) of $^{99\text{m}}\text{Tc}$ -Se NPs complex in the liver was $19.47 \pm 4\%$ at 10 min post-injection (p.i.) with merely no significant accumulation in spleen, but the expected value in stomach and lungs is about 9.4 ± 2 and $6 \pm 1\%$ at 10 min p.i. The data suggested that these radiolabeled nanoparticles are well above the size of the hydrodynamic diameters (HDs) of renal clearance threshold (< 6 to 8 nm). The activity at the kidney is around 3.8 ± 2 after 6 h p.i. suggested the excretion of nanoparticles through the urinary tract. The experiment at post 6 h showed the accumulation mainly in the liver (approx. 2.2% ID/g) and lungs (at 3.4% ID/g) and this is suggestive of the particle size of the nanoparticles. These nanoparticles may be useful for lung or liver dysfunction. The Se NPs has the advantages of enjoying a quick circulation in the blood and allow for passive targeting through the enhanced permeability and retention (EPR) effect; in addition, the nanoparticle can actively target lungs and liver through molecular interaction or affinity which will be beneficial in assessing the functionality of these organs.

Antifungal, antispurulant, and antioxidant study

It is previously mentioned that the different antifungal drugs have been used as a preventive measure for seriously ill COVID-19 patients even if they have not tested positive for fungal infection, because 50% of one-third ventilated COVID-19 patients with *Aspergillus* infections had died in intensive care unit. The excessive use of these drugs increases antifungal drug resistance and is no longer effective for fungal inhibition. In view of the public health

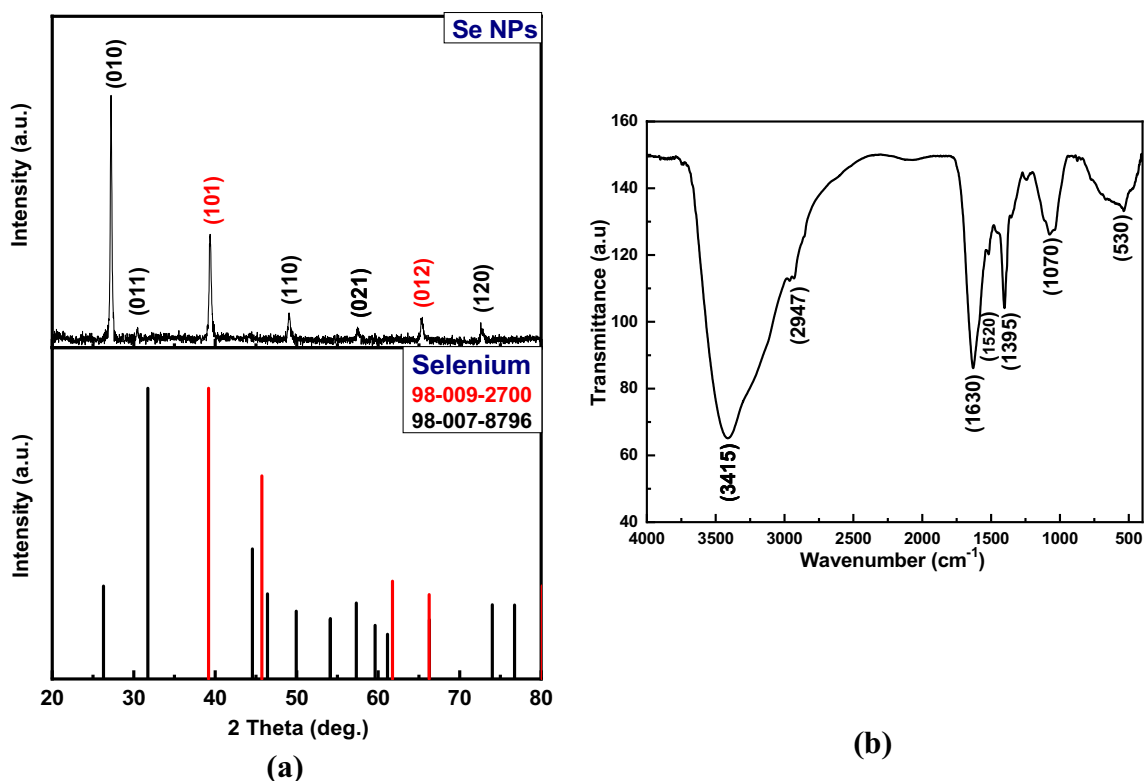


Fig. 3 **a** XRD pattern and **b** FTIR spectrum of Se NPs. XRD pattern conforming the hexagonal phase of Se NPs with space group P3121 (Ref. Pattern: 98-007-8796) and R3-MH (Ref. Pattern: 98-009-2700),

while FTIR spectrum indicating the presence of capping protein (amide I and amide II vibration)

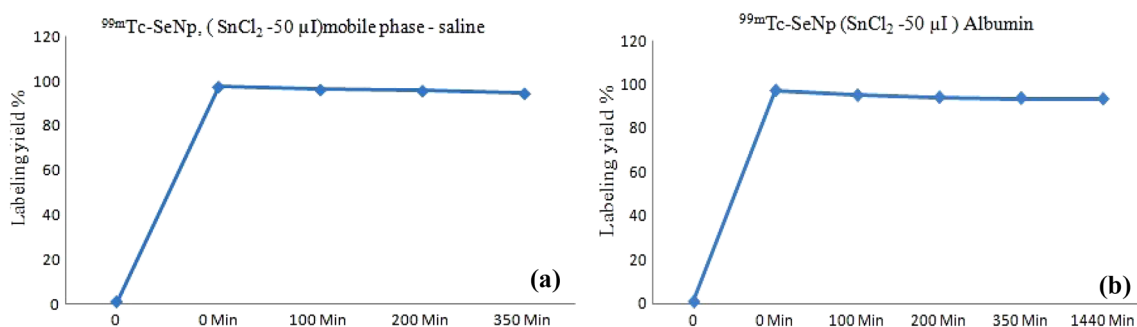
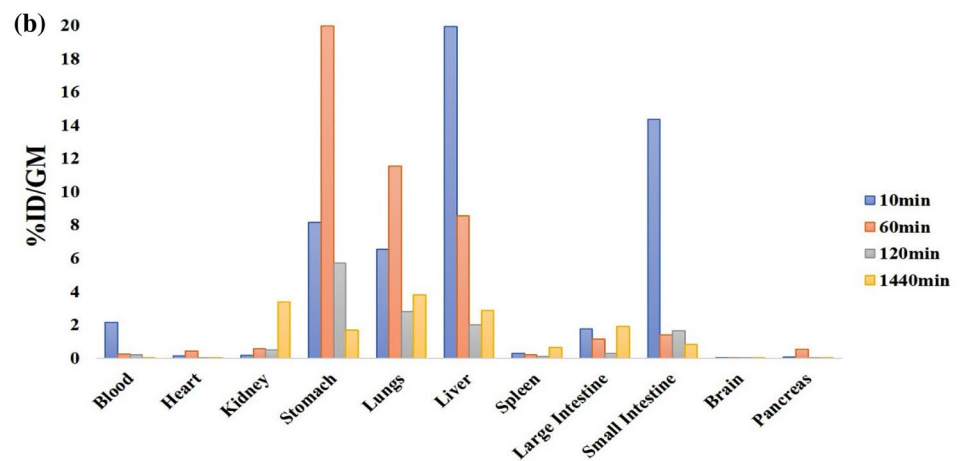
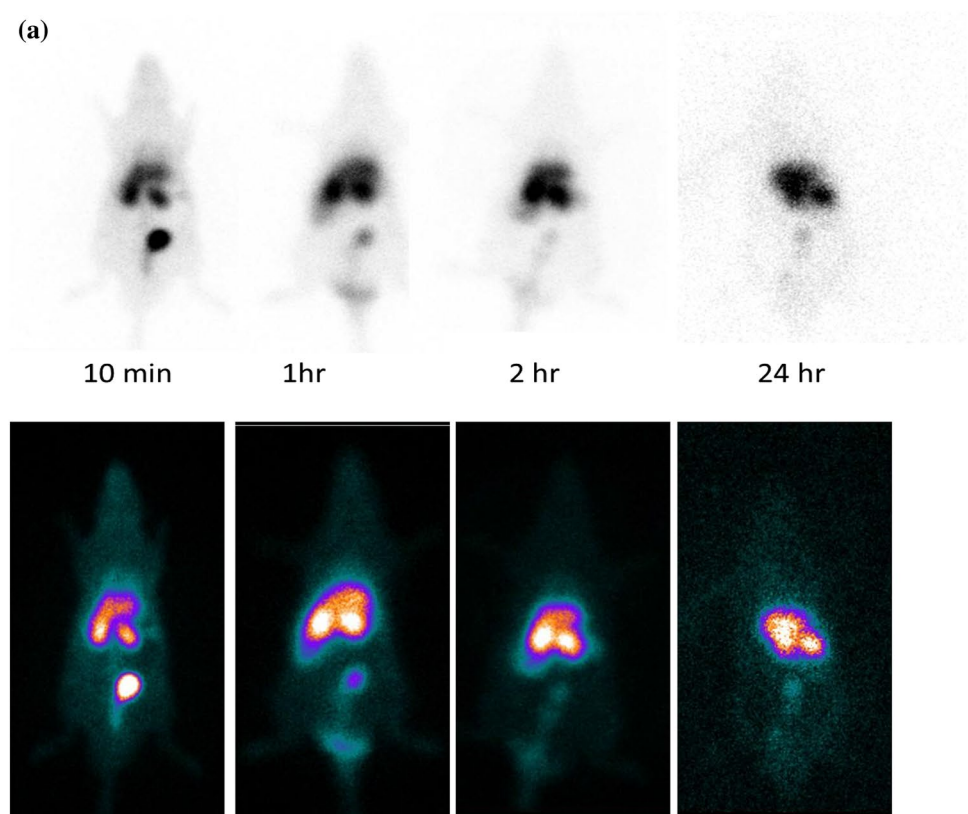


Fig. 4 Stability study of labeled nano particle at different time interval at **a** reaction solution and **b** incubated with human serum albumin at 37 °C

and current pandemic situation, our group has biosynthesized Se NPs and unveiled their antifungal and antispore activity against the black fungus *Aspergillus niger*. The antifungal activity of Se NPs was evaluated after 24, 36, and 48 h of incubation at different concentrations of 240, 120, 60, 30, 15, and 7.5 µg/30 µL (from discs A–F) against the black fungus *Aspergillus niger*. The strong antifungal activity of mycosynthesized Se NPs was ascertained by the zones of inhibition which were encircled across the sterile discs containing Se NPs (Fig. 6a). It was also observed

that the zone of inhibition increases with increasing NPs concentration. The microscopic study (Fig. 6b) showed that the aerial hyphae which contain structures (conidiophores, vesicle, metule, phialide, and conidia) for spores' production were suppressed without affecting the growth of vegetative mycelia (anti-sporulation) near inhibition boundary, while both the aerial mycelia and vegetative growth of *Aspergillus niger* were completely inhibited in the zone of inhibition (antifungal) by Se NPs. The antifungal efficiency of Se NPs was compared with standard antifungal compound (10 mcg

Fig. 5 a Single-photon emission computerized tomography images of healthy Wistar rat after 10 min, 1, 2, and 24 h of injection with ^{99m}Tc -Se NPs. **b** In-vivo biodistribution of fluorescent Se NPs in normal Wistar Rat at different time interval



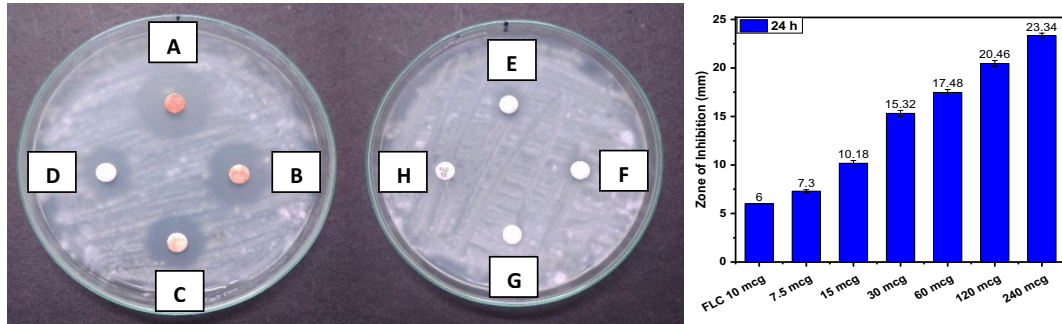
fluconazole, disc H) and the evidence indicates the potential of Se NPs to act as an effective antifungal measure against *Aspergillus niger*. In-vitro antioxidant activity of mycosynthesized Se NPs has been determined by DPPH assay. The gradual decolorization of the purple color and decrease in the absorption maxima (517 nm) of DPPH with an increase in concentration of Se NPs confirmed its antioxidant potency (Fig. 7a) which was compared with the standard antioxidant ascorbic acid (Fig. 7b). The free radical scavenging efficiency of Se NPs (1 mg/mL) was estimated (80.4%) with IC₅₀ value of 159.5 $\mu\text{g}/\text{mL}$ (Fig. 7c), while IC₅₀ value for

ascorbic acid was found to be 5.6 $\mu\text{g}/\text{mL}$ (Fig. 7d). The significant antioxidant activity of mycosynthesized Se NPs discloses its efficacy to serve as an effective antioxidant agent for various industrial and biomedical applications.

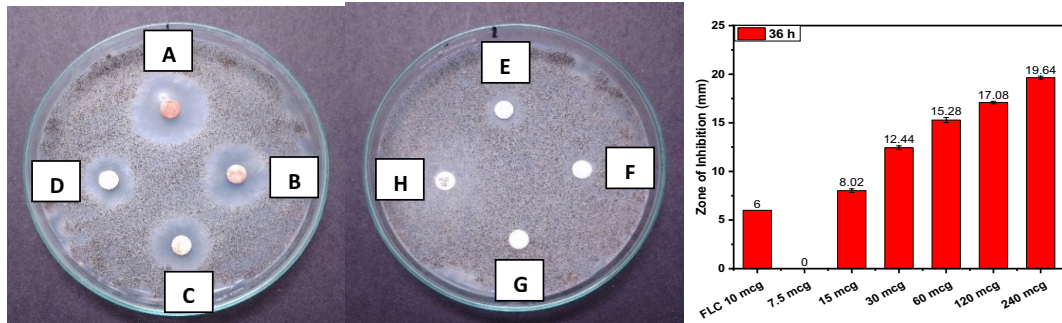
Conclusion

The present study demonstrated the potency of endophytic fungus *Fusarium oxysporum* to allow mycosynthesis of highly fluorescent, protein-capped, water dispersible Se

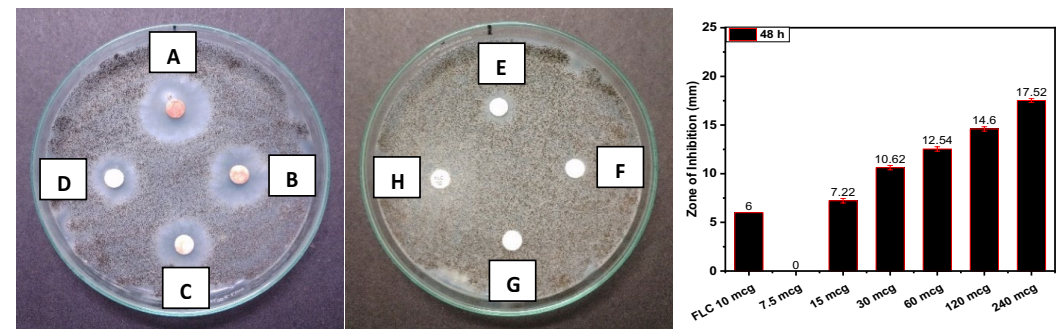
24 h



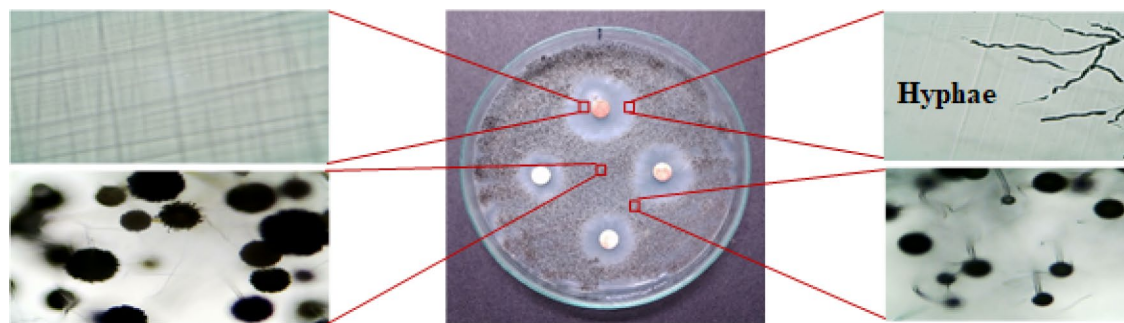
36 h



48 h



(a)



(b)

Fig. 6 a Antifungal activity of Se NPs against *Aspergillus niger* at different incubation periods of 24, 36, and 48 h. Sterile discs from A to F contain 240, 120, 60, 30, 15, and 7.5 μ g of selenium nanoparticles, while disc G is filled with double-distilled water. 10 mcg fluconazole disc (H) is used as positive control. **b** Microscopic study

suggesting antifungal and antispore activity of Se NPs against *Aspergillus niger*. The zone of inhibition and microscopic investigation clearly illustrate the antifungal and antispore efficacy of Se NPs

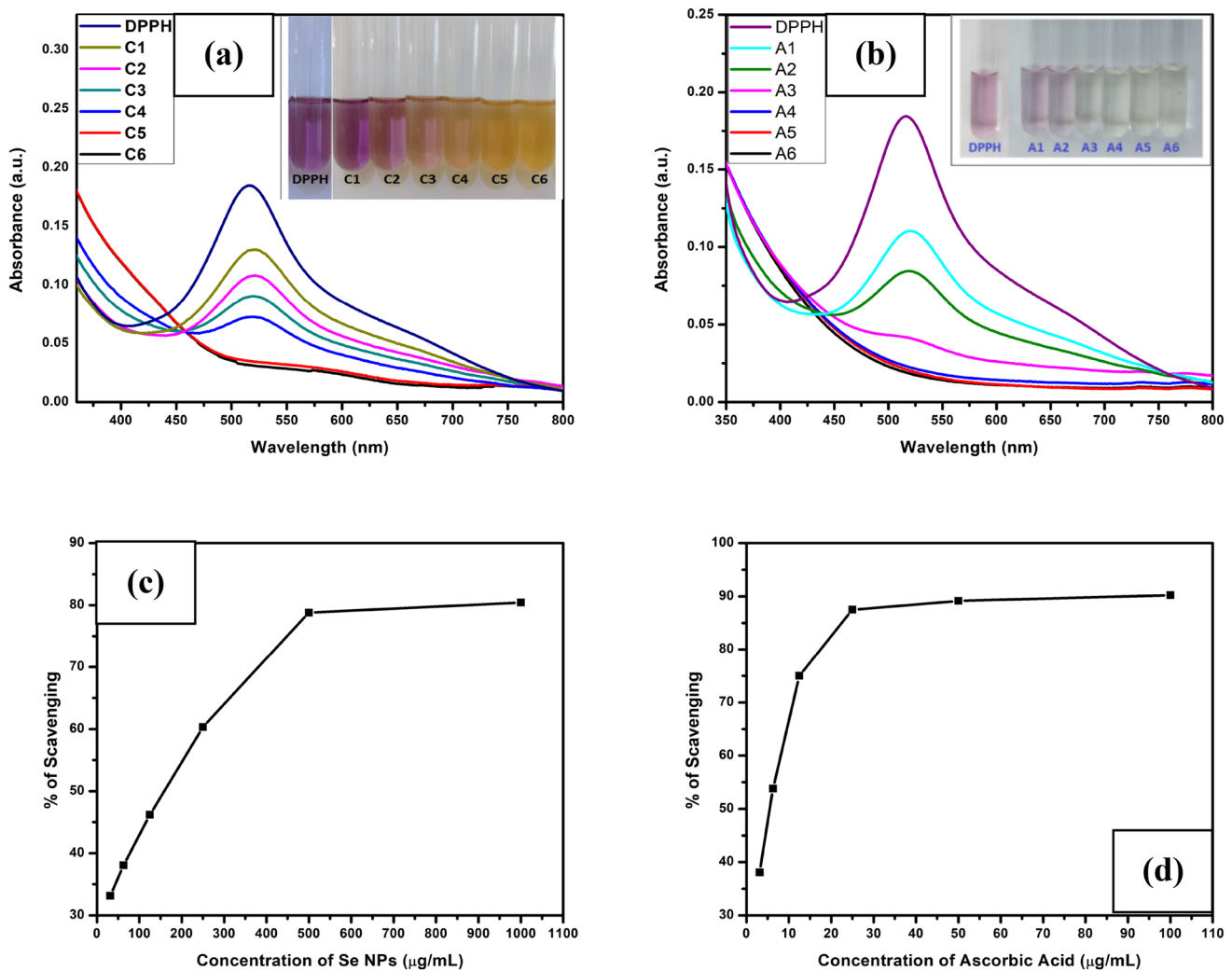


Fig. 7 UV–visible spectra of DPPH with increasing concentration of **a** selenium nanoparticles and **b** ascorbic acid. Graphical representation of DPPH free radical scavenging activity by **c** selenium nanoparticles and **d** ascorbic acid

NPs without the use of external capping agents. These spherical, crystalline Se NPs with average particle diameter of 42 nm have been fully characterized and their biodistribution, antiradical, antifungal, and antispore activity were elucidated. The biodistribution studies unfolded the influence of capping protein which determines the preferential localization of Se NPs in liver and lungs. Our mycosynthesized Se NPs also showed excellent antifungal and antispore activity against black fungus *Aspergillus niger* which has become life-threatening to SARS-CoV-2 patients during pandemic. At a time when drug resistance is rising to high levels, our mycogenic Se NPs exhibiting effective antifungal, antispore, and antioxidant activity will find major use in the development of a novel and improved drug. Since our kidneys can filter up to 50 nm in size, our mycosynthesized Se NPs can treat lung and

liver disorders and seamlessly pass through the kidneys and get expelled out of the body via urine. This will prevent selenium retention in the body, which might lead to selenium toxicity.

Acknowledgements We acknowledge the Department of Biotechnology (DBT), Government of India, for setting up a Centre of Excellence (COE, BT/PR1-3584/COE/34/29/2015) at Interdisciplinary Nanotechnology Centre (INC), Aligarh Muslim University, AMU, Aligarh, UP-202002, India. We thank Mr. Asraf Ali Khan and Mr. Alim Kazmi of INC for their technical assistance.

Funding Department of Biotechnology, Ministry of Science and Technology, India, BT/PR1-3584/COE/34/29/2015, Absar Ahmad.

Declarations

Conflict of interest The authors have no conflicts of interest in the publication.

Ethical approval The ethical standards are followed throughout the animal study and animal care standards set out by the institutional animal ethics committee (IEAEA/2018/174). They were given free access to food and drink while staying in groups of six. They were kept with a 12-h light/dim cycle at a constant room temperature.

References

- Abu-Elghait M, Hasanin M, Hashem AH, Salem SS (2021) Ecofriendly novel synthesis of tertiary composite based on cellulose and mycosynthesized selenium nanoparticles: characterization, antibiofilm and biocompatibility. *Int J Biol Macromol* 175:294–303. <https://doi.org/10.1016/j.ijbiomac.2021.02.040>
- Ahmad A, Senapati S, Khan MI et al (2003) Extracellular biosynthesis of monodisperse gold nanoparticles by a novel extremophilic actinomycete, *thermomonospora* sp. *Langmuir* 19:3550–3553. <https://doi.org/10.1021/la026772l>
- Ahmad A, Rautaray D, Sastry M (2004) Biogenic calcium carbonate: calcite crystals of variable morphology by the reaction of aqueous Ca^{2+} ions with fungi. *Adv Funct Mater* 14:1075–1080. <https://doi.org/10.1002/adfm.200400005>
- Ahmad A, Jagadale T, Dhas V et al (2007) Fungus-based synthesis of chemically difficult-to-synthesize multifunctional nanoparticles of CuAlO_2 . *Adv Mater* 19:3295–3299. <https://doi.org/10.1002/adma.200602605>
- Ashengroph M, Hosseini SR (2021) A newly isolated *Bacillus amyloliquefaciens* SRB04 for the synthesis of selenium nanoparticles with potential antibacterial properties. *Int Microbiol* 24:103–114. <https://doi.org/10.1007/s10123-020-00147-9>
- Bulgarini A, Lampis S, Turner RJ, Vallini G (2021) Biomolecular composition of capping layer and stability of biogenic selenium nanoparticles synthesized by five bacterial species. *Microb Biotechnol* 14:198–212. <https://doi.org/10.1111/1751-7915.13666>
- Chandramohan S, Naveenkumar S, Kaviyarasu K et al (2021) Biodistribution of selenium nanoparticles (SeNPs) to the Wistar rats and its breastfed offspring. *J Drug Deliv Sci Technol* 61:102299. <https://doi.org/10.1016/j.jddst.2020.102299>
- Cruz LY, Wang D, Liu J (2019) Biosynthesis of selenium nanoparticles, characterization and X-ray induced radiotherapy for the treatment of lung cancer with interstitial lung disease. *J Photochem Photobiol B Biol* 191:123–127. <https://doi.org/10.1016/j.jphotobiol.2018.12.008>
- He J, Li C, Ding L et al (2019) Tumor targeting strategies of smart fluorescent nanoparticles and their applications in cancer diagnosis and treatment. *Adv Mater* 31:1–31. <https://doi.org/10.1002/adma.201902409>
- Huang Y, Fu Y, Li M et al (2020) Chirality-driven transportation and oxidation prevention by chiral selenium nanoparticles. *Angew Chem* 132(11):4436–4444. <https://doi.org/10.1002/ange.201910615>
- Ibrahim SRM, Sirwi A, Eid BG et al (2021) Bright side of *Fusarium oxysporum*: secondary metabolites bioactivities and industrial relevance in biotechnology and nanotechnology. *J Fungi*. <https://doi.org/10.3390/jof7110943>
- Islam SN, Naqvi SMA, Parveen S et al (2021a) Application of mycogenic silver/silver oxide nanoparticles in electrochemical glucose sensing: alongside their catalytic and antimicrobial activity. *3Biotech* 11:342. <https://doi.org/10.1007/s13205-021-02888-4>
- Islam SKN, Naqvi SMA, Parveen S et al (2021b) Endophytic fungus - assisted biosynthesis, characterization and solar photocatalytic activity evaluation of nitrogen - doped Co_3O_4 nanoparticles. *Appl Nanosci* 11:1651–1659. <https://doi.org/10.1007/s13204-021-01824-5>
- Islam SN, Raza A, Naqvi SMA et al (2022) Unveiling the antispore activity of mycosynthesized gold-selenide nanoparticles against black fungus *Aspergillus niger*. *Surf Interfaces* 29:101769. <https://doi.org/10.1016/j.surf.2022.101769>
- Jung HS, Neuman KC (2021) Surface modification of fluorescent nanodiamonds for biological applications. *Nanomaterials* 11:1–23. <https://doi.org/10.3390/nano11010153>
- Khan SA, Ahmad A (2014) Enzyme mediated synthesis of water-dispersible, naturally protein capped, monodispersed gold nanoparticles; their characterization and mechanistic aspects. *RSC Adv* 4(15):7729–7734. <https://doi.org/10.1039/C3RA43888K>
- Khan SA, Gambhir S, Ahmad A (2014) Extracellular biosynthesis of gadolinium oxide (Gd_2O_3) nanoparticles, their biodistribution and bioconjugation with the chemically modified anticancer drug taxol. *Beilstein J Nanotechnol* 5:249–257. <https://doi.org/10.3762/bjnano.5.27>
- Khairalla GM, El-Deeb BA (2015) Antimicrobial and antibiofilm effects of selenium nanoparticles on some foodborne pathogens. *LWT - Food Sci Technol* 63:1001–1007. <https://doi.org/10.1016/j.lwt.2015.03.086>
- Kokila K, Elavarasan N, Sujatha V (2017) *Diospyros montana* leaf extract-mediated synthesis of selenium nanoparticles and their biological applications. *New J Chem* 41:7481–7490. <https://doi.org/10.1039/c7nj01124e>
- Korany M, Mahmoud B, Ayoub SM et al (2020) Synthesis and radiolabeling of vitamin C-stabilized selenium nanoparticles as a promising approach in diagnosis of solid tumors. *J Radioanal Nucl Chem* 325(1):237–244. <https://doi.org/10.1007/s10967-020-07195-5>
- Korde P, Ghotekar S, Pagar T et al (2020) Plant extract assisted eco-benevolent synthesis of selenium nanoparticles-a review on plant parts involved, characterization and their recent applications. *J Chem Rev* 2:157–168. <https://doi.org/10.33945/SAMI/JCR.2020>
- Kumar SA, Abyaneh MK, Gosavi SW et al (2007) Nitrate reductase-mediated synthesis of silver nanoparticles from AgNO_3 . *Biotechnol Lett* 29(3):439–445. <https://doi.org/10.1007/s10529-006-9256-7>
- Li S-D, Huang L (2008) Pharmacokinetics and biodistribution of nanoparticles. *Mol Pharm* 5:496–504. <https://doi.org/10.1021/mp800049w>
- Mellinas C, Jiménez A, Garrigós MC et al (2019) Microwave-assisted green synthesis and antioxidant activity of selenium nanoparticles using *Theobroma cacao* L. bean shell extract. *Molecules* 24:4048. <https://doi.org/10.3390/molecules24224048>
- Mukherjee P, Ahmad A, Mandal D et al (2001) Bioreduction of AuCl_4^- ions by the fungus, *Verticillium* sp. and surface trapping of the gold nanoparticles formed. *Angew Chemie - Int Ed* 40:3585–3588. <https://doi.org/10.1002/1521-3773>
- Na-bangchang K (2019) Pharmacokinetic studies of nanoparticles as a delivery system for conventional drugs and herb- derived compounds for cancer therapy : a systematic review. *Int J Nanomed* 14:5659–5677. <https://doi.org/10.2147/IJN.S213229>
- Piacenza E, Presentato A, Heyne B, Turner RJ (2020) Tunable photoluminescence properties of selenium nanoparticles: biogenic versus chemogenic synthesis. *Nanophotonics* 9:3615–3628. <https://doi.org/10.1515/nanoph-2020-0239>
- Prasanth S, Sudarsanakumar C (2017) Elucidating the interaction of L-cysteine capped selenium nanoparticles and human serum albumin: spectroscopic and thermodynamic analysis. *New J Chem* 41:9521–9530. <https://doi.org/10.1039/c7nj00477j>
- Qian F, Li X, Tang L et al (2017) Selenium quantum dots: preparation, structure, and properties. *Appl Phys Lett* 110:053104. <https://doi.org/10.1063/1.4975358>
- Sanià G, Carrese B, Lamberti A (2020) Nanoparticle surface functionalization: how to improve biocompatibility and cellular internalization. *Front Mol Biosci* 7:587012. <https://doi.org/10.3389/fmolb.2020.587012>

- Shankar SS, Ahmad A, Pasricha R, Sastry M (2003) Bioreduction of chloroaurate ions by geranium leaves and its endophytic fungus yields gold nanoparticles of different shapes. *J Mater Chem* 13:1822–1826. <https://doi.org/10.1039/b303808b>
- Sudhasree S, Banu AS, Brindha P, Kurian GA (2014) Toxicological and environmental chemistry synthesis of nickel nanoparticles by chemical and green route and their comparison in respect to biological effect and toxicity. *Environ Chem* 96(5):743–754. <https://doi.org/10.1080/02772248.2014.923148>
- Sukhanova A, Bozrova S, Sokolov P et al (2018) Dependence of nanoparticle toxicity on their physical and chemical properties. *Nanoscale Res Lett* 13:44. <https://doi.org/10.1186/s11671-018-2457-x>
- Syed A, Ahmad A (2012) Extracellular biosynthesis of platinum nanoparticles using the fungus *Fusarium oxysporum*. *Colloids Surf B Biointerfaces* 97:27–31. <https://doi.org/10.1016/j.colsurfb.2012.03.026>
- Tehrani HAM, Keyhanfar M, Behbahani M et al (2020) Synthesis and characterization of algae-coated selenium nanoparticles as a novel antibacterial agent against *Vibrio harveyi*, a *Penaeus vannamei* pathogen. *Aquaculture* 534:736260. <https://doi.org/10.1016/j.aquaculture.2020.736260>
- Vahidi H, Barabadi H, Saravanan M (2020) Emerging selenium nanoparticles to combat cancer: a systematic review. *J Clust Sci* 31:301–309. <https://doi.org/10.1007/s10876-019-01671-z>
- Wadhvani SA, Shedbalkar UU, Singh R, Chopade BA (2016) Biogenic selenium nanoparticles: current status and future prospects. *Appl Microbiol Biotechnol* 100:2555–2566. <https://doi.org/10.1007/s00253-016-7300-7>
- Wei Y, Quan L, Zhou C, Zhan Q (2018) Factors relating to the bio-distribution and clearance of nanoparticles and their effects on in-vivo application. *Nanomedicine* 13:1495–1512. <https://doi.org/10.2217/nmm-2018-0040>
- Yuan D, He H, Wu Y et al (2019) Physiologically based pharmacokinetic modeling of nanoparticles. *J Pharm Sci* 108:58–72. <https://doi.org/10.1016/j.xphs.2018.10.037>
- Zhang H, Chen S, Jia X et al (2021) Science of the total environment comparison of the phytotoxicity between chemically and green synthesized silver nanoparticles tenuated toxicity to cucumber plants. *Sci Total Environ* 752:142264. <https://doi.org/10.1016/j.scitotenv.2020.142264>

Springer Nature or its licensor holds exclusive rights to this article under a publishing agreement with the author(s) or other rightsholder(s); author self-archiving of the accepted manuscript version of this article is solely governed by the terms of such publishing agreement and applicable law.